

Azimuthal Dependence of Pion Interferometry at the AGS

M.A. Lisa⁽¹⁾, N. N. Ajitanand⁽²⁾, J. M. Alexander⁽²⁾, M. Anderson⁽³⁾, D. Best⁽⁴⁾, F.P. Brady⁽³⁾, T. Case⁽⁴⁾, W. Caskey⁽³⁾, D. Cebra⁽³⁾, J.L. Chance⁽³⁾, P. Chung⁽²⁾, B. Cole⁽⁵⁾, K. Crowe⁽⁴⁾, A.C. Das⁽¹⁾, J.E. Draper⁽³⁾, M.L. Gilkes⁽²⁾, S. Gushue^(6,2), M. Heffner⁽³⁾, A.S. Hirsch⁽⁷⁾, E.L. Hjort⁽⁷⁾, L. Huo⁽⁸⁾, M. Justice⁽⁹⁾, M. Kaplan⁽¹⁰⁾, D. Keane⁽⁹⁾, J.C. Kintner⁽¹¹⁾, J. Klay⁽³⁾, D. Krofcheck⁽¹²⁾, R. A. Lacey⁽²⁾, J. Lauret⁽²⁾, H. Liu⁽⁹⁾, Y.M. Liu⁽⁸⁾, R. McGrath⁽²⁾, Z. Milosevich⁽¹⁰⁾, G. Odyniec⁽⁴⁾, D.L. Olson⁽⁴⁾, S.Y. Panitkin⁽⁹⁾, C. Pinkenburg⁽²⁾, N.T. Porile⁽⁷⁾, G. Rai⁽⁴⁾, H.G. Ritter⁽⁴⁾, J.L. Romero⁽³⁾, R. Scharenberg⁽⁷⁾, L. Schroeder⁽⁴⁾, B. Srivastava⁽⁷⁾, N.T.B. Stone⁽⁴⁾, T.J.M. Symons⁽⁴⁾, R. Wells⁽¹⁾, J. Whitfield⁽¹⁰⁾, T. Wienold⁽⁴⁾, R. Witt⁽⁹⁾, L. Wood⁽³⁾, and W.N. Zhang⁽⁸⁾

(E895 Collaboration)

⁽¹⁾ *The Ohio State University, Columbus, Ohio 43210*

⁽²⁾ *Depts. of Chemistry and Physics, SUNY Stony Brook, New York 11794-3400*

⁽³⁾ *University of California, Davis, California, 95616*

⁽⁴⁾ *Lawrence Berkeley National Laboratory, Berkeley, California, 94720*

⁽⁵⁾ *Columbia University, New York, New York 10027*

⁽⁶⁾ *Brookhaven National Laboratory, Upton, New York 11973*

⁽⁷⁾ *Purdue University, West Lafayette, Indiana, 47907-1396*

⁽⁸⁾ *Harbin Institute of Technology, Harbin, 150001 P. R. China*

⁽⁹⁾ *Kent State University, Kent, Ohio 44242*

⁽¹⁰⁾ *Carnegie Mellon University, Pittsburgh, Pennsylvania 15213*

⁽¹¹⁾ *St. Mary's College, Moraga, California 94575*

⁽¹²⁾ *University of Auckland, Auckland, New Zealand*

(February 9, 2020)

Two-pion correlation functions, measured as a function of azimuthal emission angle with respect to the reaction plane, provide novel information on the anisotropic shape and orientation of the pion-emitting zone formed in heavy ion collisions. We present the first experimental determination of this information, for semi-central Au+Au collisions at 2-6 AGeV. The source extension perpendicular to the reaction plane is greater than the extension in the plane, and tilt of the pion source in coordinate space is found to be opposite its tilt in momentum space.

Nuclear collisions at finite impact parameter are intrinsically anisotropic with respect to the azimuthal angle about the beam direction. For nearly two decades, a growing community has studied the details of the momentum-space anisotropy of emitted particles (directed and elliptic flow) at all collision energies [1]. Theoretical studies [2–7] suggest that *coordinate-space* anisotropies are equally interesting. Recently, a formalism was proposed to use azimuthally-sensitive intensity interferometry, correlated event-by-event with the reaction plane, to extract this information experimentally [5,6]. In this Letter, we present the first experimental measurement of the full coordinate-space anisotropies of a hot nuclear source, from pions emitted from Au+Au collisions at 2-6 AGeV.

Two-particle interferometry (HBT) is the most direct probe of the space-time structure of the hot system formed in high energy heavy ion collisions [8,9], and, along with flow, the past decades have also seen extensive pion HBT measurements map out the space-time geometry and dynamics of heavy ion collisions from

Bevalac (~ 1 AGeV) energies [10], at the AGS (2-11 AGeV) [11–14], and to the highest available energy (~ 160 AGeV) at the CERN SPS [15,16]. With the exception of some recent preliminary studies [12,14,17], all experimental studies to date have assumed cylindrical symmetry of the source about the beam axis, strictly valid only for $b = 0$.

The E895 Collaboration at the AGS used a large acceptance detector to measure charged particles from Au+Au collisions. For every event, the charged particle multiplicity is used to estimate the the magnitude of the impact parameter vector $|\mathbf{b}|$, with an uncertainty ~ 0.5 fm. For all data presented here, the estimated impact parameter range is $|\mathbf{b}|=4-8$ fm. The direction of \mathbf{b} is determined from the azimuthally anisotropic momentum distribution of protons and light nuclear fragments (not pions), with an estimated uncertainty of $\sim 20 - 35^\circ$. Further details are available elsewhere [18,19].

Experimental details, such as correction for momentum resolution and particle identification, of the (azimuth-integrated) HBT analysis have been published [11,12]. Here, we discuss points particular to the azimuthally-sensitive analysis.

As in “standard” HBT analyses, correlation functions are constructed by dividing the two-pion yield as a function of relative momentum $\mathbf{q} = \mathbf{p}_1 - \mathbf{p}_2$, by a background generated by mixing pions of the current event with those of previous events [20]. As is well-known, single-particle acceptance/efficiency and phase-space effects cancel out with this “event-mixing” technique. However, there is a special consideration here. In the present analysis, we generate correlation functions with selections on the pair

angle with respect to the reaction plane $\phi = \angle(\mathbf{K}_\perp, \mathbf{b})$, where $\mathbf{K}_\perp = (\mathbf{p}_1 + \mathbf{p}_2)_\perp$ is the total momentum of the pair perpendicular to the beam [21]. Thus, we only mix events which have similar (within 5°) directions of reconstructed \mathbf{b} .

The correlation function was binned according to \mathbf{q} -components in the Bertsch-Pratt (“out-side-long”) decomposition as measured in the Au+Au c.m. frame [22]. In this Letter, we use the subscripts “o, s, l” to stand for “out, side, long.” Here, q_l is the component parallel to the beam, q_o is the component parallel to \mathbf{K} , and q_s is perpendicular to q_l and q_o . Particles in a pair were ordered such that $q_l > 0$; the signs of the other two components were retained.

Figure 1 shows two-dimensional projections of the correlation function for 4 AGeV Au+Au semicentral collisions, measured in eight 45° -wide bins in ϕ . The average rapidity and p_T of pions in low- q pairs was 1.2 (midrapidity) and 110 MeV/c, respectively, and did not vary with ϕ -bin.

Especially in the $q_o - q_l$ and $q_s - q_l$ projections, the correlation functions display a distinct “tilt,” which evolves with the emission angle ϕ . As discussed below, this tilt arises from fundamental geometry [6], in contrast to a similar tilt observed [16] in some $q_o - q_l$ projections measured far from midrapidity for azimuthally-integrated HBT, which arises from dynamic (longitudinal flow) effects [23]. Aside from these dynamical effects, there are no 2-dimensional tilts in azimuthally-integrated HBT, and only one-dimensional projections are typically shown [12].

Using a maximum-likelihood technique, we fit the correlation functions for each of the ϕ bins with the standard Gaussian parameterization [9]

$$C(\mathbf{q}, \phi) = 1 + \lambda(\phi) \exp\left[-\sum_{i,j=o,s,l} q_i q_j R_{ij}^2(\phi)\right]. \quad (1)$$

In contrast to azimuthally-integrated analyses, all six radius parameters are relevant here [5,6,9].

Two-dimensional projections of the fits, weighted according to the mixed-event background, are shown as contours in Figure 1. Since the relative sign of any component of $\mathbf{q} = \mathbf{p}_1 - \mathbf{p}_2$ is arbitrary (while the relative sign between components is not arbitrary), the two-dimensional projections in Figure 1 have been reflected for clarity. However, the fits were performed in the full three dimensions, with each pion pair being weighted only once.

Although the full structure of the correlation function is only visible in multi-dimensional projections such as those in Figure 1, one-dimensional projections are commonly shown for azimuthally-integrated HBT analyses, to provide a feeling for the quality of the data and fit. For reference, one-dimensional projections of the correlation function and fits, for one ϕ slice, are shown in Figure 2.

The seven fit parameters R_{ij} and λ are plotted as a function of ϕ in Figure 3. As is well-known [8,9], the HBT “radii” parameters are in general not strictly the radii of the emitting source, but have a geometrical interpretation as lengths of homogeneity of the emitting region. For realistic sources, various interpretations of λ have been proposed (see e.g. [24,25]). At AGS energies, the observed strong energy dependence of λ was well reproduced [11] by detailed simulations using the RQMD (v2.3) transport model [26]; there, the decrease of λ with energy was attributed to increased production of long-lived π^- -emitting particles at higher energy (see also [27]). In this scenario then, the HBT radii characterize a Gaussian “core” of directly-produced pions, with $\lambda < 1$ resulting from a well-separated “halo” of pions emitted from long-lived particles [28]. In this framework, we now discuss the ϕ -dependence of the HBT parameters, and how to extract the underlying geometry of the “core” of the source.

The ϕ -independence of λ indicates that the fraction of π^- from long-lived resonances is independent of emission angle with respect to the reaction plane. This seems reasonable, given the relatively weak anisotropic flow at these energies [18], as well as the randomizing effect on the pion from decay of the parent.

R_o and R_s show significant equal and opposite second-order oscillations in ϕ , consistent with the simple picture of a transverse profile of the pion-emitting region that reflects the “almond-shaped” overlap region (with a larger spatial extent perpendicular to \mathbf{b} than parallel to \mathbf{b}) between the target and projectile spheres [3,12].

Note that the “cross-term” radii (R_{ol}^2 , R_{os}^2 , R_{sl}^2) quantify the tilt observed in the 2-dimensional correlation function projections of each ϕ -bin of Figure 1. R_{ol}^2 and R_{sl}^2 display equal-magnitude first-order oscillations, consistent with pion emission from an ellipsoidal source which is tilted in coordinate space in the reaction plane, and away from the beam axis [6].

In general, the six HBT radii are related to the spatiotemporal structure of the emitting source via the equations [5,6]

$$\begin{aligned} R_s^2 &= S_{11} \sin^2 \phi + S_{22} \cos^2 \phi - S_{12} \sin 2\phi, \\ R_o^2 &= S_{11} \cos^2 \phi + S_{22} \sin^2 \phi + S_{12} \sin 2\phi \\ &\quad - 2\beta_\perp S_{01} \cos \phi - 2\beta_\perp S_{02} \sin \phi + \beta_\perp^2 S_{00}, \\ R_l^2 &= S_{33} - 2\beta_l S_{03} + \beta_l^2 S_{00}, \\ R_{os}^2 &= S_{12} \cos 2\phi + \frac{1}{2} (S_{22} - S_{11}) \sin 2\phi \\ &\quad + \beta_\perp S_{01} \sin \phi - \beta_\perp S_{02} \cos \phi, \\ R_{ol}^2 &= (S_{13} - \beta_l S_{01}) \cos \phi - \beta_\perp S_{03} \\ &\quad + (S_{23} - \beta_l S_{02}) \sin \phi + \beta_l \beta_\perp S_{00}, \\ R_{sl}^2 &= (S_{23} - \beta_l S_{02}) \cos \phi - (S_{13} - \beta_l S_{01}) \sin \phi. \end{aligned} \quad (2)$$

where β_\perp and β_l are the average pair velocities in the transverse and longitudinal direction, and the spatial correlation tensor $S_{\mu\nu}$ is given by

$$S_{\mu\nu} = \langle \tilde{x}_\mu \tilde{x}_\nu \rangle, \quad \tilde{x}_\mu = x_\mu - \bar{x}_\mu, \quad (\mu, \nu = 0, 1, 2, 3) \quad (3)$$

where the brackets $\langle \rangle$ indicate an average over the emitting source. In Equations 2, $\mu = 3$ refers to the beam direction, and $\mu = 1$ is parallel to \mathbf{b} .

Simultaneously fitting the six $R_{ij}^2(\phi)$ of Figure 3 with Equations 2 (treating the $S_{\mu\nu}$ as 10 ϕ -independent fit parameters) allows extraction of the full spatial correlation tensor

$$S = \begin{pmatrix} 13.4 \pm 3.5 & 0.7 \pm 0.9 & 0.2 \pm 1.0 & 0.0 \pm 1.1 \\ 0.7 \pm 0.9 & 21.3 \pm 0.9 & -0.1 \pm 0.6 & 4.5 \pm 0.6 \\ 0.2 \pm 1.0 & -0.1 \pm 0.6 & 25.5 \pm 1.0 & -0.3 \pm 0.6 \\ 0.0 \pm 1.1 & 4.5 \pm 0.6 & -0.3 \pm 0.6 & 22.8 \pm 0.9 \end{pmatrix}$$

where all units are in fm^2 and $c = 1$. The fits are shown by solid lines in Figure 3.

The only significantly non-vanishing tensor elements are the diagonal ones $S_{\mu\mu}$ and S_{13} . This fact, along with observations of identical oscillation amplitudes in R_o^2 and R_s^2 , and in R_{ol}^2 and R_{sl}^2 , support the assumption of ϕ -independence of $S_{\mu\nu}$ in the fit [5,6].

S_{13} and $(S_{22} - S_{11})$ quantify, respectively, first and second harmonic oscillations of the HBT radii with respect to the measured reaction plane. However, due to finite particle multiplicity, the measured reaction plane differs statistically from the true one by some angle $\Delta\phi$ [18,29]. This reaction plane dispersion results in an apparent reduction in both S_{13} and $(S_{22} - S_{11})$ (but does not affect quantities S_{00} , S_{33} , and $(S_{11} + S_{22})$). According to [5,29,30]

$$S_{13,m} = S_{13} \cdot \langle \cos(\Delta\phi) \rangle \quad (4)$$

$$(S_{22} - S_{11})_m = (S_{22} - S_{11}) \cdot \langle \cos(2\Delta\phi) \rangle, \quad (5)$$

where $S_{13,m}$ is the observed value, and S_{13} is the “true” value. The correction factors obtained by following the procedure outlined in Refs. [5,18,19,29] are listed in Table I. Hence, for the 4 AGeV data, the reaction plane-dispersion corrected values are $S_{11} = 19.8 \pm 1.2$, fm^2 , $S_{22} = 27.0 \pm 1.4$ fm^2 , and $S_{13} = 5.2 \pm 0.7$ fm^2 .

The spatial tilt of the emission ellipsoid in coordinate space is given by [6]

$$\theta_s = \frac{1}{2} \tan^{-1} \left(\frac{2S_{13}}{S_{33} - S_{11}} \right) = 37^\circ \pm 4^\circ. \quad (6)$$

Rotating the spatial correlation tensor (corrected for reaction-plane dispersions) by this angle returns the diagonal tensor

$$R_y^\dagger(\theta_s) \cdot S \cdot R_y(\theta_s) = \begin{pmatrix} 13.4 \pm 3.5 & 0.5 \pm 1.0 & 0.2 \pm 1.0 & 0.4 \pm 1.0 \\ 0.5 \pm 1.0 & 15.9 \pm 1.0 & 0.1 \pm 0.6 & 0.0 \pm 0.9 \\ 0.2 \pm 1.0 & 0.1 \pm 0.6 & 27.0 \pm 1.4 & -0.3 \pm 0.6 \\ 0.4 \pm 1.0 & 0.0 \pm 0.7 & -0.3 \pm 0.6 & 26.8 \pm 0.8 \end{pmatrix}$$

whose diagonal elements are the squared lengths of homogeneity ($S_{\mu\mu} = \sigma_\mu^2$) in the t, x, y, z directions.

Similar results are obtained at other energies. Figures 4 and 5 show the HBT parameters obtained at 2 and 6 AGeV [31,32]. Especially at the highest energy, degraded reaction-plane resolution significantly reduces the second-order oscillations in the transverse radii. Considered in isolation, R_o^2 in Figure 5 may be fit by a constant (ϕ -independent) value as well as anything else. However, the simultaneous fit of all $R^2(\phi)$ allows relatively clean extraction of the source shape parameters. Reaction plane dispersion corrections are applied to all data, but the effects are small. For the worst case (6 AGeV dataset), the corrections result in a decrease (increase) in σ_x (σ_y) of 0.3 fm, and 5° reduction in θ_s ; σ_z and σ_t are unchanged.

Table II summarizes the inferred pion source shapes for our three energies. At all energies, our results indicate a pion freezeout distribution as an ellipsoid whose major axis in the reaction plane is tilted with respect to the beam in the positive direction (i.e. in the direction of \mathbf{b}), and whose transverse axis perpendicular to the reaction plane is longer than the axis in the reaction plane (the “almond” shape referred to above). The extension in the temporal direction is consistent with observations at high energy [11,13,15,16].

The observed transverse “almond” shape is reminiscent of the entrance channel geometry. In the simplest picture, pions are emitted from the overlap region of the two spherical Au nuclei. For impact parameter $b = 4$ fm (8 fm), the spatial RMS of the overlap region is 2.2 fm (1.3 fm) parallel to \mathbf{b} , and 2.9 fm (2.4 fm) perpendicular [33]. While the linear scale of the freezeout distribution is roughly twice these estimates (see Table II), indicating significant expansion, the aspect ratio $\sigma_y/\sigma_x \approx 1.3 - 1.4$, is in the range (1.3 - 1.9) expected from this naive picture.

On the other hand, the large positive tilt is a geometric feature of the collision dynamics [6]. Studies with the RQMD model indicate that most of the low- p_T pions arise from Δ decay, so it is not surprising that the tilted freeze-out distribution resembles the baryonic distribution in coordinate space calculated in transport codes [4].

Experimental access to this level of geometric detail on the freezeout distribution is unprecedented, and represents an exciting new opportunity to study the dynamical response of hot nuclear matter to compression. A detailed theoretical discussion is beyond the scope of this Letter, but we note that an identical analysis on pions generated by the RQMD model displays considerable sensitivity on the dynamical effect of the nuclear meanfield; RQMD values are listed in Table II. Although the spatial scale is underpredicted at the lower energies and the temporal scale overpredicted (noted already for central collisions [11]), qualitatively, the model reproduces the “almond” shape and large positive tilt angles remark-

ably well. Since the model better describes proton directed flow when the mean field is included in the calculation [19], it is interesting to note that the tilt angles (the spatial counterpart of proton directed flow [6]) reproduce observation better when the mean field is off.

We stress that these coordinate-space anisotropies represent new information, independent of momentum-space anisotropies (directed and elliptical flow). Momentum-space tilt angles (flow angles [34]) at these energies are only a few degrees [19], and, indeed, the directed flow (momentum-space tilt) of pions at these energies is in the *negative* direction [35,36,6], opposite the coordinate-space tilt θ_s . Experimental information on the interplay between coordinate and momentum space anisotropies should help resolve theoretical issues, such as the coexistence of flow and antflow components at these energies [4].

Further studies of the elliptical transverse shape of the source at higher energy should prove quite interesting. It is known, for example, that the elliptic flow of nuclear matter (protons and pions) in *momentum space* changes sign at AGS energies [36,18,37,38], from negative (more momentum out-of-plane) at low collision energy to positive. The coordinate-space analogue of negative elliptic flow is the “almond” shape we observe. The degree to which this shape follows the momentum space and evolves to an in-plane shape at high energies, may provide valuable information on the detailed nature and cause of elliptic flow [39]; RQMD predicts [40] that the “almond” shape is retained even at RHIC energies.

In conclusion, we have presented the first full measurement of the azimuthal dependence of pion interferometry. For semi-peripheral Au+Au collisions at 2-6 AGeV, the spatial correlation tensor, $S_{\mu\nu}$, extracted from the ϕ -dependences of the HBT radius parameters, reveals an ellipsoidal pion emission region with an “almond” transverse profile and which is strongly tilted in the reaction plane away from the beam axis. Consistency relations indicate that the extracted geometry is negligibly affected by possible transverse space-momentum correlations. The RQMD transport model reproduces the qualitative features of the data quite well, and reveals a dependence of the coordinate-space anisotropies on the action of the nuclear meanfield. Through application of this new type of analysis at other energies and careful theoretical comparisons, it is hoped that fresh insight on the dynamics of non-central heavy ion collisions may be gained.

M.A.L. thanks Drs. U. Heinz, A. Poskanzer, S. Voloshin, and U. Wiedemann for important suggestions and discussions, and Drs. S. Pratt and H. Sorge for the use of their computer codes RQMD and CRAB.

This work supported by the U.S. Department of Energy under contracts DE-AC03-76SF00098 and DE-AC02-98CH10886, and grants DE-FG02-89ER40531, DE-FG02-88ER40408, DE-FG02-87ER40324 and DE-

FG02-87ER40331; by the U.S. National Science Foundation under grants PHY-98-04672, PHY-97-22653, PHY-96-01271, PHY-96-05207, and INT-92-25096; by the University of Auckland Research Committee, NZ/USA Cooperative Science Programme CSP 95/33; and by the National Natural Science Foundation of P.R. China under grant number 19875012.

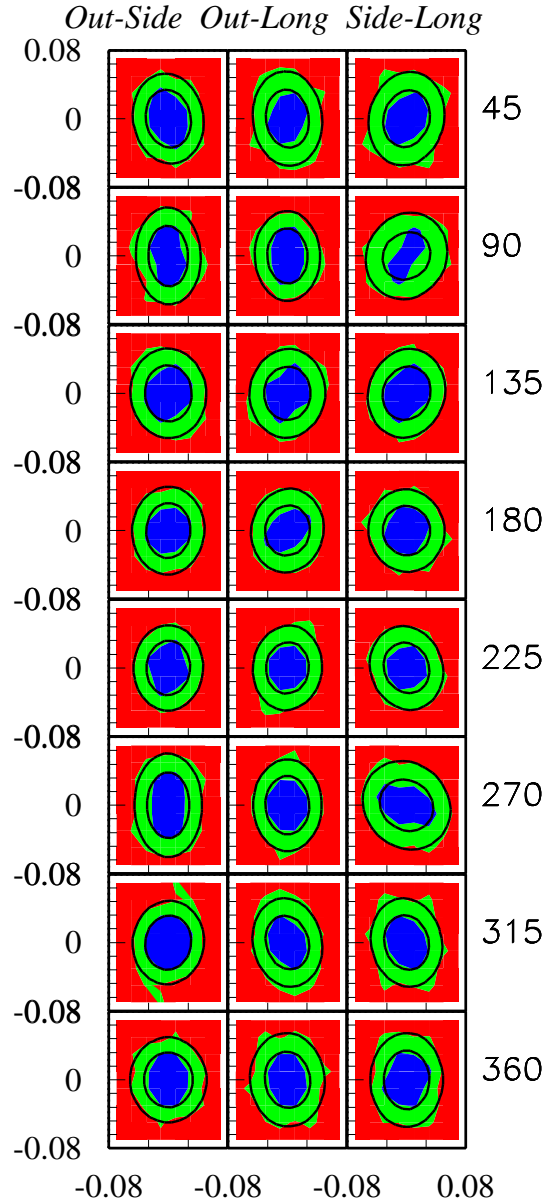


FIG. 1. Two-dimensional projections in $q_o - q_s$ (left column), $q_o - q_l$ (center column), and $q_s - q_l$ (right column), of the correlation functions measured for midrapidity pions from semi-central Au+Au collisions at 4 AGeV. For each projection, the unplotted component is integrated over ± 30 MeV/c. Indicated by the labels on the right, projections are shown for emission angles with respect to the reaction plane $\phi = 45^\circ \pm 22.5^\circ$ (top row) to $\phi = 360^\circ \pm 22.5^\circ$ (bottom row). Solid lines show projections of fits with Equation 1.

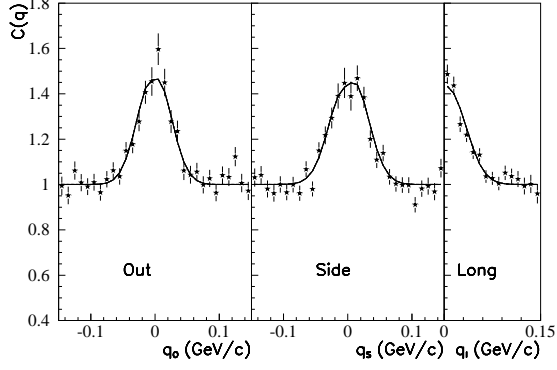


FIG. 2. One-dimensional projections, in q_o , q_s , and q_l , of the correlation function for $\phi = 45^\circ \pm 22.5^\circ$ (top row of Figure 1). For each projection, the unplotted q components are integrated over ± 30 MeV/c. Note that in the present analysis, q_l is defined positive, while q_o and q_s have a meaningful sign. Solid lines show projections of fits with Equation 1.

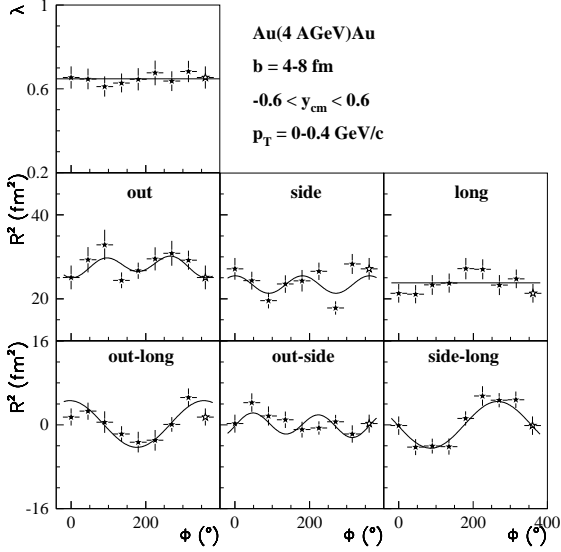


FIG. 3. Filled stars show the fit parameters from Equation 1, resulting from fits to the correlation functions of Figure 1. The values at $\phi = 0^\circ$ are redisplayed as open stars at $\phi = 360^\circ$. The line in the λ panel represents the average value of λ . Lines in the other panels represent the fit to the HBT radii (stars) with the Equation 2. The vertical scale is linear in all panels.

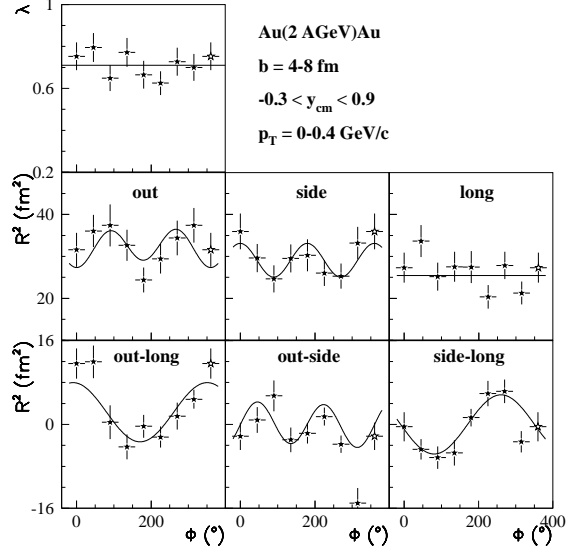


FIG. 4. Same as Figure 3, but for 2 AGeV collisions.

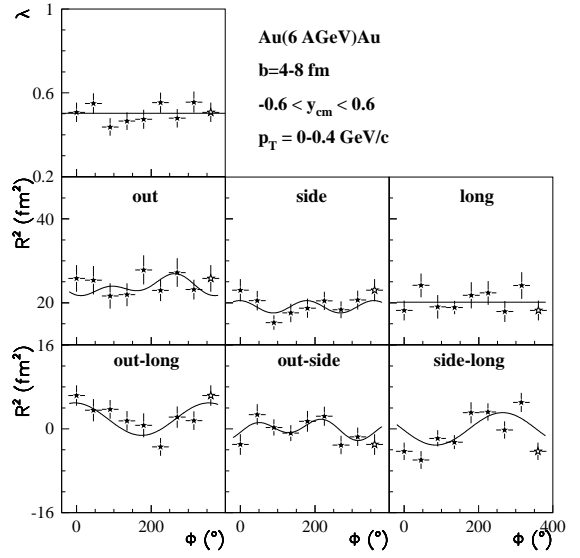


FIG. 5. Same as Figure 3, but for 6 AGeV collisions.

E (AGeV)	$\langle \cos(\Delta\phi) \rangle$	$\langle \cos(2\Delta\phi) \rangle$
2	0.940	0.787
4	0.853	0.584
6	0.724	0.384

TABLE I. First and second harmonic reaction plane dispersion correction factors for the three datasets discussed.

E (AGeV)	σ_t (fm/c)	σ_x (fm)	σ_y (fm)	σ_z (fm)	θ_s ($^\circ$)
2 Data	3.5 ± 1.0	4.2 ± 0.2	5.8 ± 0.2	5.4 ± 0.1	47 ± 5
RQMD cs	6.6 ± 0.2	2.9 ± 0.1	4.4 ± 0.1	4.4 ± 0.1	49 ± 2
RQMD mf	5.4 ± 0.2	3.1 ± 0.1	5.0 ± 0.1	4.6 ± 0.1	64 ± 2
4 Data	3.7 ± 0.5	4.0 ± 0.1	5.2 ± 0.1	5.2 ± 0.1	37 ± 4
RQMD cs	6.4 ± 0.2	3.3 ± 0.1	4.2 ± 0.1	4.7 ± 0.1	33 ± 3
RQMD mf	4.6 ± 0.3	3.5 ± 0.1	4.7 ± 0.1	4.7 ± 0.1	45 ± 3
6 Data	3.8 ± 0.5	3.5 ± 0.2	4.8 ± 0.2	4.7 ± 0.1	33 ± 6
RQMD cs	5.9 ± 0.2	3.5 ± 0.1	4.3 ± 0.1	4.9 ± 0.1	28 ± 3
RQMD mf	5.0 ± 0.3	3.6 ± 0.1	4.7 ± 0.1	4.5 ± 0.1	48 ± 5

TABLE II. Lengths of homogeneity σ_μ and tilt angle at each collision energy. In addition to experimental results, predictions of the RQMD model with meanfield off (cs) and on (mf) are given.

-
- [1] W. Reisdorf and H.G. Ritter, *Annu. Rev. Nucl. Part. Sci.* **47**, 663 (1997); N. Herrmann, J.P. Wessels, and T. Wienold, *ibid* **49**, 581 (1999).
- [2] D. Teaney and E.V. Shuryak, *Phys.Rev.Lett.* **83** (1999) 4951-4954
- [3] H. Heiselberg, *Phys. Rev. Lett.* **82**, 2052 (1999); H. Heiselberg, A.-M. Levy, *Phys. Rev. C* **59**, 2716 (1999).
- [4] J. Brachmann *et al*, *Phys.Rev.* C61 (2000) 024909; *ibid*, *nucl-th/9912014*.
- [5] U.A. Wiedemann, *Phys. Rev. C* **57**, 266 (1998).
- [6] M.A. Lisa, U. Heinz, and U.A. Wiedemann, *Phys. Lett. B* **489**, 287 (2000); *nucl-th/0003022* (2000).
- [7] S.A. Voloshin and W.E. Cleland, *Phys.Rev.* **C53** 896 (1996); S.A. Voloshin and W.E. Cleland, *Phys.Rev.* **C54** 3212 (1996).
- [8] W. Bauer, C.K. Gelbke, and S. Pratt, *Ann. Rev. Nucl. Part. Sci.* **42**, 77 (1992); U. Heinz and B. Jacak, *Ann. Rev. Nucl. Part. Sci.* **49**, 529 (1999).
- [9] U.A. Wiedemann and U. Heinz, *Phys. Rep.* **319**, 145 (1999).
- [10] S.Y. Fung *et al.*, *Phys. Rev. Lett.* **41**, 1592 (1978); A.D. Chacon, *et al.*, *Phys. Rev.* **C43**, 2670 (1991); W.B. Christie, *et al.*, *Phys. Rev.* **C47**, 779 (1993).
- [11] E895 Collaboration, M.A. Lisa *et al.*, *Phys. Rev. Lett.* **84**, 2798 (2000).
- [12] E895 Collaboration, M.A. Lisa, *et al.*, *Quark Matter '99*, *Nucl. Phys.* **A661**, 444c (1999);
- [13] E877 Collaboration, J. Barrette *et al.*, *Phys. Rev. Lett.* **78**, 2916 (1997).
- [14] E877 Collaboration, D. Miskowiec *et al.*, *Quark Matter '95*, *Nucl. Phys.* **A590** 473c (1995).
- [15] NA44 Collaboration, I.G. Bearden, *et al.*, *Phys. Rev.* **C58**, 1656 (1998).
- [16] R. Ganz, *et al.* (NA49 Collaboration), *Proceedings of CRIS'98*, S. Costa, S. Albergo, A. Insolia, and C. Tuvè, eds., p102 World Scientific (1999).
- [17] E917 Collaboration, B. Holzman, *et al*, in *Advances in Nuclear Dynamics 5*, *Proceedings of the 15th Winter Workshop on Nuclear Dynamics*, W. Bauer and G.D. Westfall, eds. Kluwer Academic Press, (1999); WA98 Collaboration, Shunji Nishimura, *et al*, *ibid*; E895 Collaboration, M.A. Lisa, *et al*, *ibid*;
- [18] C. Pinkenburg, *et al*, (E895 Collaboration) *Phys. Rev. Lett.* **83**, 1295 (1999).
- [19] H. Liu, *et al*, (E895 Collaboration) *Phys. Rev. Lett.* **84**, 5488 (2000).
- [20] G.I. Kopylov, *Phys. Lett.* **B50**, 472 (1974).
- [21] Selecting instead on $\phi_{1,2} = \angle(\mathbf{p}_{1,2}, \mathbf{b})$ yields results similar to those we discuss. However, one loses pair statistics from pairs which straddle cut borders in ϕ .
- [22] S. Pratt, *Phys. Rev.* **D33** 1314 (1986); G. Bertsch, *et al.*, *Phys. Rev.* **C37** 1896 (1988).
- [23] S. Chapman, P. Scotto, and U. Heinz, *Phys. Rev. Lett.* **74** 4400 (1995).
- [24] S. Nickerson, T. Csörgő, and D. Kiang, *Phys. Rev.* **C57** 3251 (1998).
- [25] D. Hardtke and S. Voloshin, *Phys. Rev.* **C61** 024905 (2000).

- [26] H. Sorge, Phys. Rev. C **52**, 3291 (1995).
- [27] J.P. Sullivan, *et al.*, Nucl. Phys. **A566**, 531c (1994).
- [28] T. Csörgő, Phys. Lett. **B409** 11 (1997).
- [29] S. Voloshin and Y. Zhang, Z. Phys. **C70**, 665 (1996). J.-Y. Ollitrault, nucl-ex/9711003 v2; A.M. Poskanzer and S.A. Voloshin, Phys. Rev. **C58**, 1671 (1998);
- [30] S. Voloshin, private communication.
- [31] For the 2 AGeV analysis, our rapidity cut is centered somewhat forward of midrapidity, for statistics and acceptance reasons; hence, S_{03} does not vanish [23], resulting in a net offset in $R_{oi}^2(\phi)$.
- [32] In the 6 AGeV case, the fit produces an additional non-zero component: $S_{02} = 1.3 \pm 1.0$. This results in the slight asymmetry that is clear in the fit lines to R_o^2 and R_{os}^2 . We do not consider significant this barely-nonvanishing component.
- [33] Recall that the RMS values are significantly less than the hard-sphere radius of 7 fm For a uniformly-filled hard sphere of radius R , the RMS in any one direction is $R/\sqrt{5}$.
- [34] M. Gyulassy, K.A. Frankel, and H. Stöcker, Phys. Lett. **110B**, 185 (1982); H.A. Gustafsson, *et al.*, Phys. Rev. Lett. **52** 1590 (1984).
- [35] EOS Collaboration, J. Kintner *et al.*, Phys. Rev. Lett. **78**, 4165 (1997); E895 Collaboration, G. Rai, *et al.*, Quark Matter '99, Nucl. Phys. A661, 162c (1999).
- [36] W. Caskey, Ph.D. thesis, University of California at Davis (1999)
- [37] D. Brill, *et al.*, Phys. Rev. Lett. **72** 336 (1993).
- [38] E877 Collaboration, J. Barrette, *et al.*, Nucl. Phys. **A661**, 329c (1999); *ibid*, 198c (1999).
- [39] P. Danielewicz, *et al.*, Phys. Rev. Lett. **81**, 2438 (1998).
- [40] J. Yang, *et al.*, submitted for publication (2000).